ISTITUTO NAZIONALE DI FISICA NUCLEARE

Laboratori Nazionali di Frascati

INFN-20-08/LNF
26 Giugno 2020

First characterisation of the PADME electromagnetic calorimeter

Gabriele Piperno[1] for the PADME collaboration
[1)] *Dip. di Fisica, Univ. Sapienza Roma, INFN Sezione di Roma, I-00185 Roma, Italy*

Abstract

The PADME experiment, hosted at the LNF Beam Test Facility, is searching for a dark photon that decays into dark matter particles. This search is performed looking for the reaction $e^+ + e^- \rightarrow A' + \gamma$, where A' is the dark photon, which cannot be observed directly or via its decay products. A key role in the experiment is played by the electromagnetic calorimeter, which measures the energy and the position of the γ in the final state. From this, the missing four-momentum carried away by the A' can be evaluated and the particle mass can be inferred. This article will present the process followed for the construction and calibration of the electromagnetic calorimeter of the experiment. The results achieved in terms of equalisation, detection efficiency and energy resolution during the first phase of the experiment, demonstrate the effectiveness of the various devices used to improve the calorimeter performance with respect to first prototypes.

PACS:11.30.Er,13.20.Eb;13.20Jf;29.40.Gx;29.40.Vj

Published by
Laboratori Nazionali di Frascati

1 Introduction

A possible explanation of the elusiveness of Dark Matter (DM) is that it interacts with Standard Model (SM) particles only by means of a mediator. Among the possible mediators, the Dark Photon (DP) is one of the best motivated. One of the simplest DP models, known as kinetic mixing, introduces a new U(1) symmetry which implies the existence of a new vector boson mediator, namely the A' [1, 2]. SM particles are neutral under this new symmetry, but the A' could interact with them faintly thanks to a mixing with the ordinary photon. The intensity of this interaction is given by an effective charge εq, where q is the electric charge of the particle and $\varepsilon\alpha_{e.m.}$ is the DP coupling constant to the SM. In this simple model, the DP is completely described by ε and its mass $m_{A'}$.

In addition, depending on the model, the DP could partially or completely explain the discrepancy between measurements and theory of the muon anomalous magnetic moment [3] (kinetic mixing has been discarded as the only explanation of this difference [4, 5]) and the results known as the ^{8}Be and ^{4}He anomalies [6, 7].

References [8] and [9] present a more complete DP scenario, the various experimental approaches and the current research status.

2 The PADME experiment

The Positron Annihilation into Dark Matter Experiment (PADME) is hosted at the Beam Test Facility of the Laboratori Nazionali di Frascati, in Italy [10, 11]. It looks for a DP produced via the reaction:

$$e^+ + e^- \to A' + \gamma.$$

The positrons, accelerated at $550\,\text{MeV}$ by the laboratory's LINAC, impinge on the electrons of an active diamond target of $100\,\mu\text{m}$ thickness, which gives average information about the beam position and intensity [12]. The adopted experimental technique relies on the measurement of the missing mass in the final state, which is due to the A' that leaves the detector unseen. Knowing the initial conditions, given by an electron at rest ($\underline{P}_{e^-}$) and a $550\,\text{MeV}$ positron ($\underline{P}_{e^+}$), and measuring the photon in the final state ($\underline{P}_{\gamma}$), by means of a granular electromagnetic calorimeter (ECal), it is possible to measure $m^2_{A'}$ as the square of the missing mass M_{miss}:

$$m^2_{A'} = M^2_{miss} = \left(\underline{P}_{e^+} + \underline{P}_{e^-} - \underline{P}_{\gamma}\right)^2$$

where the notation $\underline{P}$ indicates the relativistic four-momentum of each particle. The beam energy allows $m_{A'}$ to be probed up to $23.7\,\text{MeV}$. It is important to underline that this experimental approach is almost independent of the specific theoretical model selected to describe the DP, requiring only that it interacts with leptons.

In addition to the target and ECal, the setup consists of a magnetic dipole, to deflect the beam out of the calorimeter; a charged particle veto system (made of a positron veto,

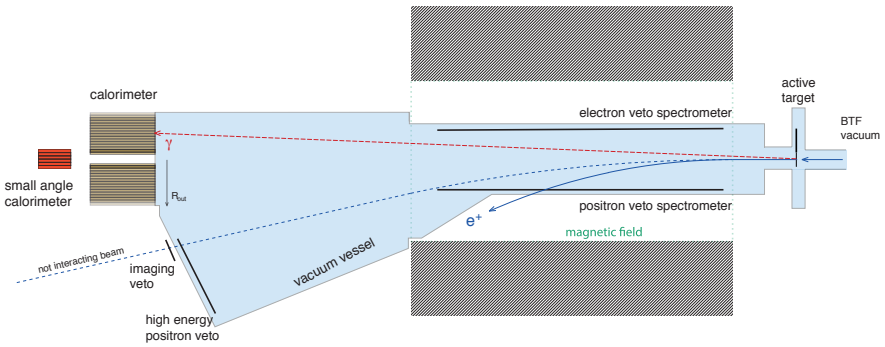

Figure 1: The PADME detector seen from above, not to scale. From right to left: the active target, the dipole magnet, with the e^+/e^- vetoes inside, the high energy positron veto and the TimePix3 array both at the beam exit and, 3.463 m away from the target, the electromagnetic calorimeter and, behind it, the small angle calorimeters.

an electron veto and a high energy positron veto [13, 14]), to identify $e^+ + e^- \to e^+ + e^-$ events and positrons that loose part of their energy through Bremsstrahlung, and lastly, a fast Small Angle Calorimeter (SAC) [15], which is able to sustain the rate of Bremsstrahlung photons in the forward direction. A schematic of the detector is shown in fig.1.

With this design, a DP event would appear as a single photon energy deposit in the ECal and nothing else in the vetoes and in the SAC.

A more detailed description of the PADME concept can be found in [16].

3 The PADME electromagnetic calorimeter

Together with the active target, the ECal is a key component of the experiment, since it is fundamental to evaluate the four-momentum of the recoil photon, measuring its energy and its impact position. The segmented calorimeter was built reshaping crystals recovered from the endcaps of the electromagnetic calorimeter of the L3 experiment [17]. The following sub-sections present first the production of the Scintillating Units (SUs), i.e. the assembly made by a crystal and its PhotoMultiplier Tube (PMT), and then introduce the calorimeter itself, together with its signal digitisation and trigger systems.

3.1 Scintillating units production

As a first step, the old reflective paint and photodiodes were removed from the original L3 crystals. To recover possible performance deterioration due to radiation damage, such as transparency loss, crystals then underwent an accelerated annealing at LAB 27 at CERN. The procedure was as follows:

1. the crystals were heated from room temperature up to 200 °C over 3 h;

2. they were kept at constant temperature at $200\,°\text{C}$ for $6\,\text{h}$;

3. finally they were cooled from $200\,°\text{C}$ to room temperature by switching off the oven, in about 1 day.

A measurement was performed to check the new transparency. The cut from the original truncated pyramid shape of the crystals, from the projective L3 calorimeter barrel, to a square face parallelepiped was performed at Gestione SILO (Italy) [18]. The same firm also performed the PMT gluing, using the ELJEN EJ-500 optical cement [19], and the crystal coating, with three layers ($\approx 60\,\mu\text{m}$) of ELJEN EJ-510, a bright white diffusive paint with titanium dioxide pigments [20].

The PMTs used are a revised version of the HZC XP1911 type B [21], whose quantum efficiency at $480\,\text{nm}$, the BGO maximum emittance wavelength, is 21% and whose dimensions ($19\,\text{mm}$ in diameter) matches very well the square face of the crystals. The gain curve of each PMT was studied before the gluing, by means of a blu led flashing in front of the glass window. The curve is obtained varying the PMT HV and measuring the tube response.

3.2 The detector

The ECal consists of 616 bismuth germanate (BGO) crystals, each of $2.1 \times 2.1 \times 23.0\,\text{cm}^3$, arranged in a cylindrical shape of $\approx 29\,\text{cm}$ external radius with a central square hole of 5×5 crystals. Since the maximum gap of the PADME magnet is $23\,\text{cm}$, and the target has to be placed sufficiently far from the magnet poles in order to minimize the deflection of the incoming beam due to the fringe field, the maximum photon angle is $\approx 100\,\text{mrad}$, which however does not reduce the DP acceptance significantly.

The size of the calorimeter is then chosen by compromising between acceptance and angular resolution. Given the practical limit to the lateral size of the detector (the number of needed crystals scales with the square of the radius), the larger the distance the smaller the coverage. In any case the maximum distance of the calorimeter from the target is limited by the available length in the experimental hall to a maximum of $\approx 4\,\text{m}$.

Considering its current distance from the target of $3.463\,\text{m}$ and its diameter, the ECal angular coverage is in the interval $[15.66, 82.11]\,\text{mrad}$, while the SAC covers the region $[0, 18.92]\,\text{mrad}$. These angles are defined by the radii of the minimum and maximum circumferences completely contained within each calorimeter.

The ECal main requirements are a small Moliére radius for a good spatial resolution and an energy resolution of the order of $2\%/\sqrt{E}$. Given the opportunity to reuse crystals from the L3 experiment and that BGO fulfills these conditions [17], the choice was made to use this material.

The size of the crystals' square faces has been chosen to leave some free space around the glued light detector, without worsening the granularity and the energy and position resolutions of the detector. This is to allow mechanical operations on single units

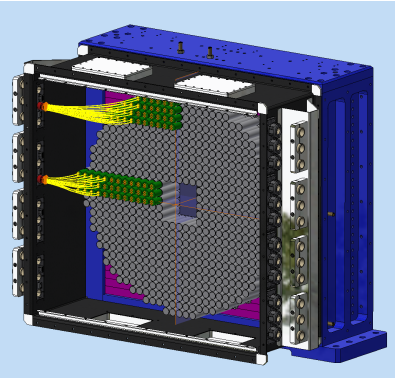

Figure 2: CAD drawing of the ECal, seen from the back and without the rear closing panel. The blue structure is the mechanical support, while the black is the cover of the PMTs and their cables. PMT dividers and cables (HV and signal) are shown only for few units. The purple components are the plastic fillers (see text for more details).

and to avoid an excessive heating of the system. The longitudinal dimension of the crystal was chosen to maximise the shower containment and corresponds to slightly more than 20 radiation lengths, being $X_0 = 1.118\,\text{cm}$ for the BGO.

The central square hole is needed to let forward Bremsstrahlung radiation pass and be detected by the SAC. The high rate of small-angle Bremsstrahlung photons would indeed flood the inner ECal crystals. The SAC is an additional, fast calorimeter, based on Cherenkov radiation, has a signal duration of about $3\,\text{ns}$ and is able to sustain particle rates up to hundreds of MHz, more than 100 times higher than the ECal. In fact 10% of the BGO scintillation light has a decay time of $60\,\text{ns}$, while that of the remaining 90% employs $300\,\text{ns}$ [22].

Since the beginning of PADME operations in October 2018, only 4 SUs did not work properly (0.65% of the total). Currently, there are plans to recover these channels for future data acquisitions.

A scheme of the calorimeter is presented in fig.2. The metal support structure has a square shape due to ease of assembly. The remaining free space between the frame and the crystals is filled with plastic elements. This also puts BGO in contact with low density material instead of metal. All the HV and signal cables exit from the rear of the ECal in groups of 64, passing through two holders, the inner of which is light-tight.

Due to the relatively small energies released in the calorimeter, SUs are not inserted in a rigid honeycomb structure, since this would have spoiled the energy resolution as a consequence of the large dead space between crystals. In assemblying the calorimeter without any holding structure, it is of fundamental importance to control the differences with respect to the nominal crystals' size. In order to have a flat surface on which layers of crystals are piled one on top of the other, two precautions were taken: crystals were individually selected on the basis of their actual transverse dimensions and $50\,\mu\text{m}$ black Tedlar® strips were used to compensate gaps between crystal heights.

With the aim of reducing the light crosstalk, Tedlar® has been inserted as vertical

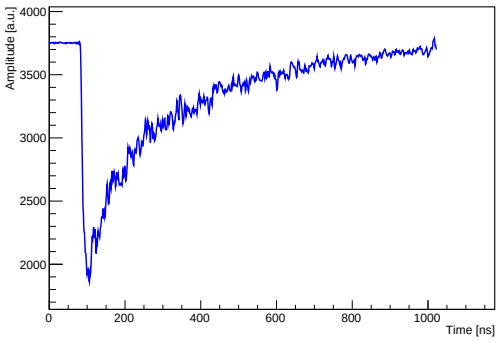

Figure 3: A typical ECal signal digitised with a sampling frequency of 1 GS/s.

strips between crystals of the same layer and as horizontal foils between consecutive layers. Additionally, to improve the energy resolution, SUs on each layer have been placed with the least well performing ones at the borders of the calorimeter and the best ones where the majority of the photons are expected.

3.3 Signal readout and trigger

The ECal analog signals are digitised using CAEN V1742 boards [23, 24]. These boards host 4 DRS4 ASICs, a switched-capacitor array sampling chip, providing a total of 32 channels. Each channel has a dynamic range of 1 V with a 12-bit precision. Due to the PMT negative signals, the voltage interval used is $[-1, 0]$ V. A single channel of the board has 1024 capacitors that continuously sample the analog input with a selectable frequency of 1 GS/s, 2.5 GS/s or 5 GS/s. The selected one is 1 GS/s, to obtain a long enough digitisation window able to match the long decay time of the BGO scintillation light. Fig.3 shows a typical pulse.

In every digitised signal there are some samples before the leading edge of the pulse. This pre-pulse region is needed to evaluate the charge collected by the SU, as described in sec.4.2, which in turn is proportional to the energy deposited by an interacting particle. During the PADME data-taking, the number samples in the pre-pulse varies depending on the type of trigger.

A Cosmic Ray (CR) trigger is provided by two scintillating slabs, positioned one above and one under the ECal (see sec.4.2 for more details). The beam trigger signal is generated by the accelerator complex for each bunch. It has a digitally adjustable delay (in 1 ns steps), which allows the synchronisation with the experiment data acquisition.

The number of the pre-pulse samples in the CR case is ≈ 100, while it ranges from ≈ 200 to ≈ 400 in the beam trigger condition, due to a bunch length of about 200 ns. As a consequence, there are always 2 or 3 decay times for a pulse in an acquired window. Since the integral of the charge is used as indication of the energy release in the crystal, this variability is taken into account and corrected for in the offline analysis.

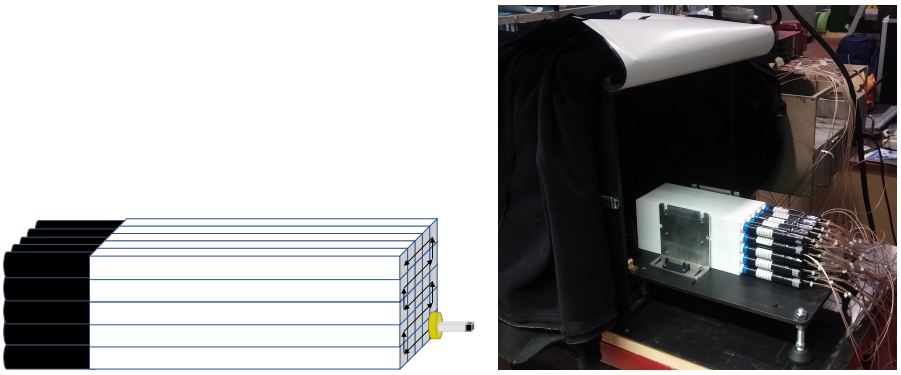

Figure 4: Setup for SU calibration. Left: scheme of the test stand (image not to scale), with the ^{22}Na source indicated with a yellow disk, whose movements are also drawn; a LYSO crystal is placed on the opposite side of the source to provide the trigger signal. Right: a photograph of the real test stand, where the SUs are visible.

4 Scintillating unit calibration and equalisation

The SUs were calibrated by means of a ^{22}Na source before being mounted in the calorimeter. This was done in order to determine the charge vs HV curve and to set the SU voltages to get the desired pC/MeV gain. Starting from the middle of November 2018, the CR trigger was also implemented to check the response of the units to minimum ionizing particles (MIPs). Using this type of event it is possible to validate the ^{22}Na calibration and to assess and improve the equalisation of the SUs. In the following the relative results of the process are presented.

4.1 Pre-assembly calibration with ^{22}Na

To select and to equalise the response of each SU, a dedicated setup was built, exploiting the two back-to-back $511\,\text{keV}$ photons emitted by a ^{22}Na source. This setup was used in the pre-assembly phase to characterize all the SUs: it allows to scan a 5×5 SU matrix, with the source moving in front of each crystal. Fig.4 left shows a drawing with the sodium path highlighted, while in fig.4 right there is a photograph of the test stand. A $3 \times 3 \times 20\,\text{mm}^3$ LYSO crystal readout by a SiPM, placed in front of the source on the opposite side with respect to the BGO, constitutes the trigger: when a photon is detected, the signal of the facing SU is taken, regardless of its content. SUs are measured at 10 different voltages in the interval $[1100, 1550]\,\text{V}$, in steps of $50\,\text{V}$, acquiring about 5000 events per HV value.

An example of the charge distribution obtained for a unit at $1400\,\text{V}$ is presented in fig.5 left: the pedestal and the $511\,\text{keV}$ signal are clearly visible and both are fitted with a Gaussian, while the approximately flat continuum is taken into account using a constant function.

For each event, charge is evaluated as the integral of the corresponding pulse. Integrals are obtained considering the area between the pulse and a flat line, which, in

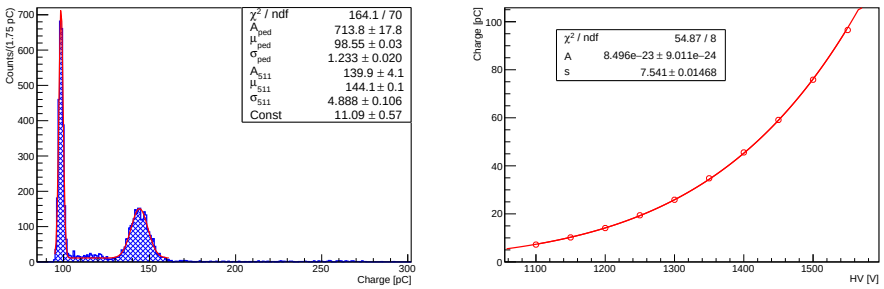

Figure 5: Left: charge distribution of a SU at $1400\,\mathrm{V}$ with a double Gaussian plus a flat function to fit the pedestal, the $511\,\mathrm{keV}$ peak and the constant background; see the text for the pedestal offset explanation. Right: Charge as a function of the HV with the gain curve fit of the kind $Q = A \cdot V^s$ superimposed, with Q charge, V voltage and A and s fit parameters; only statistical errors are shown.

general is not the pulse baseline. Therefore pedestals are generally not peaked at zero, as in fig.5 left. Using all the distributions for a given SU and evaluating the charge as the difference between the $511\,\mathrm{keV}$ peak position and the pedestal position, it is possible to determine the charge as a function of the HV. Fig.5 right presents the gain behaviour with the best fit curve superimposed, for the same SU as fig.5 left. This is of the form $Q = A \cdot V^s$, where Q is charge, V voltage and A and s are free parameters. Exploiting these curves and the knowledge that the peak energy is $511\,\mathrm{keV}$, it is possible to perform the ECal pC/MeV equalisation.

In fig.6 the distribution of the voltages needed to obtain a gain of $15.3\,\mathrm{pC/MeV}$ is displayed, for each of the 616 PADME SUs. The distribution mean is $1186\,\mathrm{V}$ with a standard deviation of approximately $53\,\mathrm{V}$, meaning that the units' variability is small. Even the largest value, $1411\,\mathrm{V}$, is well below the safety operational maximum of $1700\,\mathrm{V}$ [21]. The gain is chosen to be at the centre of the linearity range of the PMTs and to ensure a complete containment for signals with an energy of $1\,\mathrm{GeV}$, which is almost two times the beam energy. This possibility is taken into account because several photons may release their energy in the same crystal at the same time.

To evaluate the reproducibility of the calibration results, 135 SUs (22% of the total) underwent a second, identical, measurement campaign. Performing a fit on this second data set and requiring the same gain equalisation, it is possible to obtain a second voltage to compare with the first one. The relative difference between the two HVs, given by $\frac{V_1 - V_2}{(V_1+V_2)/2}$, shows changes that always remain below a few percent, as visible in fig.7. This difference also incorporates the variation due to the day/night temperature and sunlight environmental fluctuations, which are not kept completely under control in the test area, in contrast to the experimental hall where the detector is installed.

To keep the calibration under control during the next period of data-taking, the ECal will be equipped with an automated system that is capable of positioning a ^{22}Na source in front of each crystal.

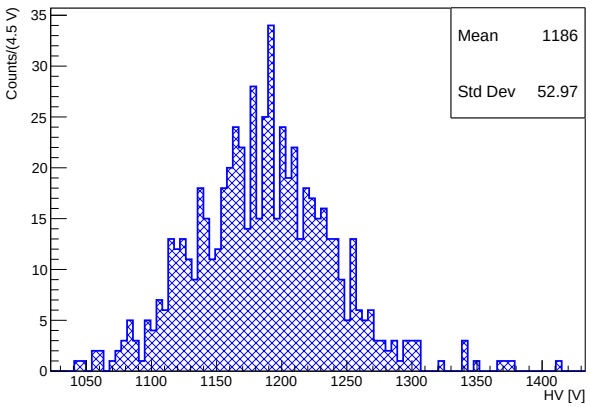

Figure 6: Distribution of the PMT voltages to set the corresponding SU at $15.3\,\mathrm{pC/MeV}$.

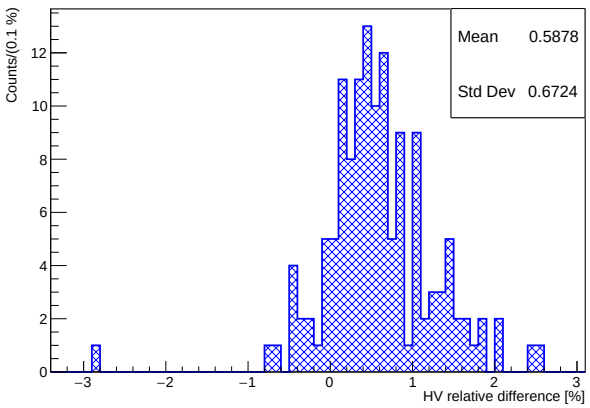

Figure 7: Relative difference between the first and the second voltage value for the 135 SUs that were tested a second time to check the gain curve reproducibility. The required gain is $15.3\,\mathrm{pC/MeV}$ in both cases.

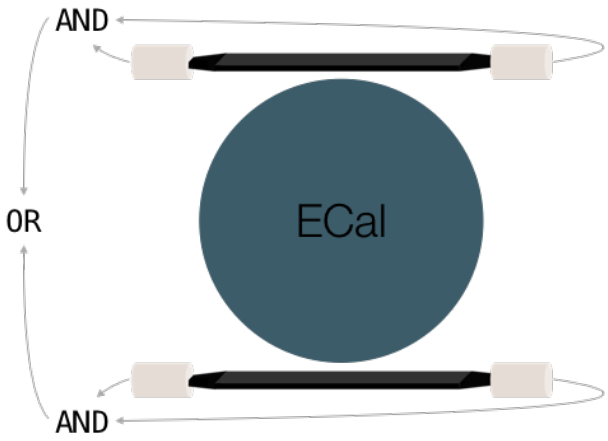

Figure 8: Structure and logic of the ECal CR trigger. It consists of two plastic scintillator slabs, one above and one below the ECal. Each bar is read by a couple of PMTs, one per side, set in logic AND. The logic OR of the two ANDs gives the trigger signal.

4.2 Cosmic rays

After the calibration, all the SUs were assembled to build the ECal. Since the start of data taking, the calorimeter has been operated with voltages corresponding to a gain of 15.3 pC/MeV. As shown in fig.8, the calorimeter is equipped with a CR trigger, made by two plastic scintillator slabs, one above and one below the ECal, both read by two PMTs (one per side). The PMTs on the same slab are set in logic AND. To increase the event rate and to include CRs which traverse the ECal diagonally and cross a single slab, the trigger is given by the logic OR of the two ANDs. Being monolithic bars, the position where the CR crosses a BGO crystal is not known.

Fig.9 gives an example of a CR passing through the whole calorimeter. Here, the numbers in the various positions indicate the charge collected by each SU.

Studying the charge distribution obtained from CRs in the various SUs, it is possible to check the calorimeter equalisation resulting from the selected HVs. To have a more precise evaluation, only CRs crossing a crystal vertically are considered. The verticality is defined by the fulfillment of three conditions:

- the passage of a CR through three SUs aligned in a column;
- no other signal in the three rows which the considered three SUs belong to;
- only the pulse coming from the central SU of the three is considered for the calculation.

This ensures that the CR releases no energy in adjoining crystals. For example in fig.9 only SUs in position $(15, 21)$ and $(20, 9)$ respect these requirements. For peripheral units with no SU directly above or below (68, corresponding to 11% of the total, see white SUs in fig.11 left) the two crystals below or above are used, respectively.

Contrary to the situation of the ^{22}Na source, in the case of CRs there are no triggered empty events with which to build the pedestal peak, as shown in fig.5 left. Consequently,

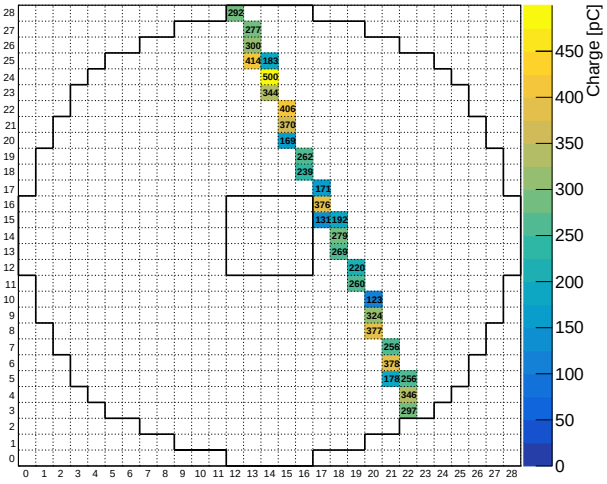

Figure 9: A cosmic ray passing through the ECal. The color scale and the numbers inside the squares represent the charge collected by the SU.

the charge is evaluated subtracting from the mean of the first 50 pre-pulse samples each sample amplitude (pulses are negative, as shown in fig.3) and then summing over all the samples.

Fig.10 presents an example of the Most Probable Values (MPVs) coming from Landau fits performed on charge distributions of SUs for data taken over three days, when these are crossed vertically by CRs. On the left there is the 2D distribution, with a colour scale and the value inside each cell, while on the right there are two superimposed histograms: one in blue, considering all the active SUs and one in red, excluding the 68 with no units on top of or below them. The means of the two Gaussian fits are compatible, being (266.3 ± 1.4) pC for all of the SUs and (266.0 ± 1.4) pC for the innermost ones. Taking into account the Gaussian for all the units, the ECal equalisation achieved using the gain curves from the ^{22}Na source corresponds to $(10.99 \pm 0.48)\%$.

The left plot of fig.10 also shows in white the positions of the 4 non-working channels. If one of these belongs to the triplet of crystals needed for the condition of verticality, it is skipped and the one above or below is used.

As a result of this study it is also possible to improve the calorimeter energy resolution. Assuming that, on average, CRs release the same amount of energy in all the crystals, the MPVs of the charge distribution can be used as a normalisation term, simply dividing each pulse integral by the MPV of the corresponding ECal channel.

CRs are also used to evaluate the efficiency of the SUs. Performing calculations exclusively with pulses that passed the zero-suppression (approximately 1 MeV threshold), ensures that only signals from CRs are used. Using the same triplets defined in the previous analysis, the central SU efficiency is evaluated by checking if a signal is present when the crystals above and below have one. Efficiency is given by the ratio between the number of times all the three cells have an occurrence and the number of times only the

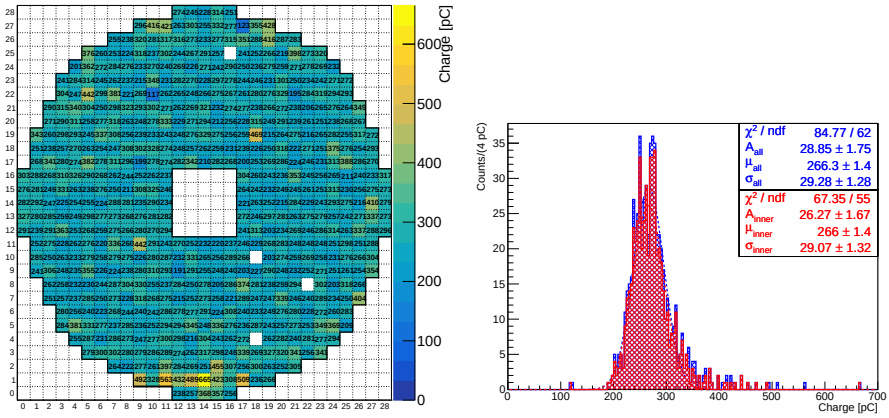

Figure 10: Examples of MPVs obtained from the Landau fits to the charge distributions of SUs when considering only CRs passing vertically through them (see text for verticality definition). Left: 2D distribution of values across the ECal; this plot highlights the presence of 4 non-working SUs. Right: MPV distributions considering (blue) and not considering (red) the 68 crystals with no other units above or below them, with Gaussian fits; the two distributions are well in agreement (in both the 4 non-working SUs are not included).

two external ones have it.

Due to its evaluation algorithm, efficiency is estimated only for internal SUs, because it is not possible to measure it with the same accuracy for channels on the ECal borders. Fig.11 left shows the 2D distribution of ECal efficiencies, represented by a colour scale and a value inside each cell, for a CR data taken over three days. Units with no number are the excluded ones. In fig.11 right there is the histogram of the measured efficiencies with a zoom in the interval $[97, 101]\%$ in a inset. A reverse Landau fit is superimposed on both distributions, given by the formula $A \cdot \mathcal{L}(\frac{-\varepsilon+\text{MPV}}{\sigma})$, where A is the amplitude, $\mathcal{L}$ the Landau (with its MPV and σ) and ε the efficiency. Efficiency on photons is expected to be similar to the one obtained with muons, which are MIPs and approximately release energies in the interval $[15, 30]$ MeV.

With reference to fig.11 right, fig.12 reports the cumulative of the SUs as a function of the efficiency. Percentage is given not considering the four non-working units and the 68 on the border.

4.3 Calorimeter tests with BTF positron beam

Several tests were performed on a prototype of 5×5 crystals of dimensions $2.0 \times 2.0 \times 22.0\,\text{cm}^3$ (slightly smaller than the final ones), before the ECal construction. In particular, single positron beams of different energies were fired on the central crystal of the matrix. These measurements showed an energy resolution in line with the desired performance, being $\frac{\sigma(E)}{E} = \frac{2.0\%}{\sqrt{E[\text{GeV}]}} \oplus \frac{0.003\%}{E[\text{GeV}]} \oplus 1.1\%$ [25]. The experimental points (red and blue squares) together with the fit line are presented in fig.13. Here, blue squares identify

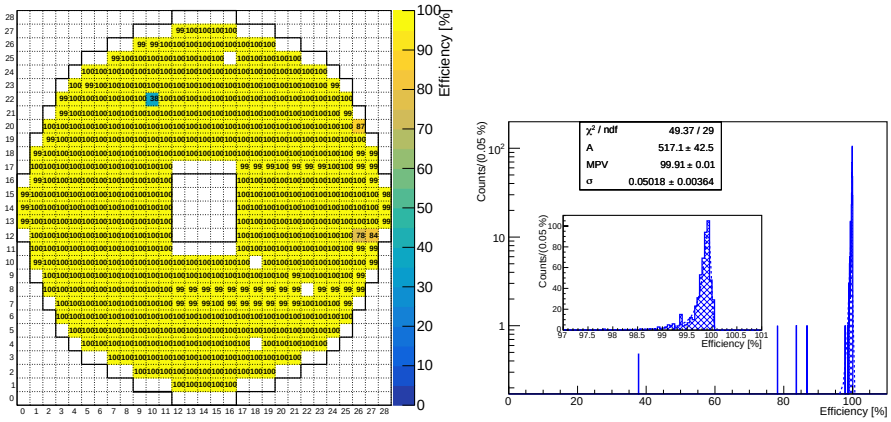

Figure 11: Efficiency of SUs, evaluated using CR data taken over three days, after applying a selection on the charge, which corresponds to a minimum energy of about $1\,\mathrm{MeV}$. Left: 2D distribution across the ECal. Right: efficiency distribution with a reversed Landau fit superimposed (see text); in the inset there is a zoom in the region $[97, 101]\%$. In both graphics neither the 4 non-working units nor the 68 ones that doesn't have a crystal above or below are included.

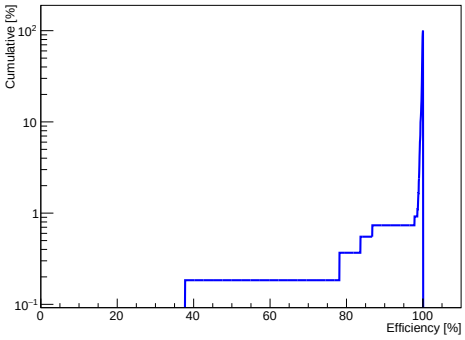

Figure 12: Cumulative in $\%$ of the efficiency distribution of fig.11. The percentage of the cumulative is given not considering the four non-working units.

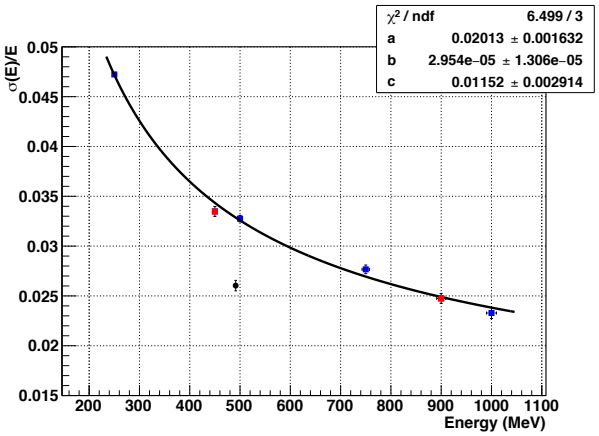

Figure 13: Energy resolution of the prototype, given by the squares and the black fit line (from [25]), compared to the ECal results, indicated with a black circle. The two colours for the squares identify results coming from beams of different energies: blue for 250 MeV (single and multiple) positrons, red for 450 MeV (single and multiple) positrons.

results produced using a 250 MeV beam, while red squares identify results produced with a beam of 450 MeV. Furthermore, the test showed that for particles of energy up to 1 GeV the discrepancy from linearity always remains within 2%. Since its gain is comparable to that of the prototype and its PMTs have a larger gain linearity interval with respect to the ones used for the test matrix, an improved linearity is expected for the ECal.

The effectiveness of the procedure explained in sec.4.2 for the energy resolution was tested firing a 490 MeV positron beam of multiplicity ≈ 1 directly on the calorimeter. To have comparable results, a 5×5 cluster around the crystal with the largest energy deposit was again considered, to simulate the prototype condition (other clusterisation algorithms implemented for PADME are given in [26]). At this energy, the resolution improved, becoming $(2.62 \pm 0.05\,(\text{stat}))\%$, as shown by the black circle in fig.13.

Furthermore, during this test, the probability of having multiple photons in the same SU is higher that in the standard condition, since the beam is directed always to the same region of the ECal. This lead to a spoiling of the energy resolution, due to a worse pulse charge evaluation in a multi-interaction environment with respect to the single-interaction condition. Consequently, an additional improvement in energy resolution during normal data taking is expected.

Apart from a more refined analysis, the reasons for such an improvement in the energy resolution has two origins: the SUs development and the beam optimisation (beam related components are not factorised from the ECal ones).

Relatively to the SUs, in addition to the smaller dimensions of the crystals, which have a lower energy containment, there are other important differences that make the prototype ones perform less well with respect to the final ones:

- PMTs were different and not optimised (HZC XP1912 instead of the revised HZC

XP1911);

- PMTs were connected to the BGO by means of optical grease (not glued);
- crystals were wrapped with two layers of PTFE tape (not painted);
- SUs were not equalised, with a voltage of 1100 V for all of them.

Concerning the beam, it contributes to the measured energy resolution, with different factors for the two cases. The beam used for the prototype test was not as optimised as in the ECal case. In order to have the possibility to change the energy during the test-beam, secondary electrons were produced on the BTF target from the LINAC primary beam. This is necessary because the primary beam has a well defined energy, needed for the DAΦNE operations. Consequently, to obtain electrons of a certain energy, the beam is sent towards a target and then particles with the desired energy and charge are selected between the emerging ones by means of a dipole. In addition, because of the DAΦNE collider operations, the primary LINAC beam was switching between electrons and positrons production, with different parameters, at intervals of about 10 minutes.

Conversely, in the ECal test the beam was an optimisated primary beam consisting only of 490 MeV positrons. Moreover, in this second case the LINAC gun was off and only few electrons were accelerated (the ones produced by the gun dark current in phase with the accelerating field), while in the prototype case the primary beam was consisting of approximately 10^9 particles.

This extreme reduction in the number of primary accelerated particles and the absence of a conversion target allowed for a significant diminution of the energy deposited in the calorimeter thanks to the disappearance of the background photons produced at the BTF target. In turn, this reflected in an improvement of the ECal energy resolution.

5 Conclusions

The PADME experiment is designed to search for a dark photon (A') that decays into dark matter particles, possibly produced in the reaction $e^+ + e^- \to A' + \gamma$. The experimental approach is based on the missing mass technique: knowing the initial kinematics and measuring the final photon four-momentum, by means of an electromagnetic calorimeter, it is possible to evaluate the A' mass, consequently the electromagnetic calorimeter represents one of the most important components of the experiment and its energy calibration is of fundamental importance.

This article reviews each step followed during the construction of the PADME electromagnetic calorimeter, from the initial L3 experiment crystal recovery and annealing to the final assembly of the 616 scintillating units. The trigger and the DAQ system are contextually described.

Energy calibration was performed individually for each unit by means of a ^{22}Na source, exploiting its back-to-back 511 keV photons. During data taking the gain was

set to $15.3\,$pC/MeV, at the centre of the linearity response interval. In data taken over three days the resulting overall ECal equalisation and the scintillating unit efficiency were $(10.99 \pm 0.48)\%$ and $\geq 98\%$ for 99.1% of the channels, respectively.

Finally, to check the effect of the calibration and equalisation on the energy resolution, a measurement was performed directing a $490\,$MeV positron beam of multiplicity ≈ 1 directly on the calorimeter. The obtained resolution is $(2.62 \pm 0.05\,(\text{stat}))\%$, an evident improvement with respect to the calorimeter prototype result at the same energy, demonstrating the effectiveness of the various procedures here described.

References

[1] P. Galison and A. Manohar, Phys. Lett. B **136** (1984) 279

[2] B. Holdom., Phys. Lett. B **166** (1986) 196

[3] M. Pospelov 2009 Phys. Rev. D **80** 095002

[4] M. Ablikim *et al.*, Phys. Lett. B **774** (2017) 252

[5] J. P. Lees *et al.*, Phys. Rev. Lett. **119** (2017) 131804

[6] A. J. Krasznahorkay *et al.,* Phys. Rev. Lett. (2016) **116** 042501

[7] A. J. Krasznahorkay *et al.* arXiv: 1910.10459 (2019)

[8] M. Raggi and V. Kozhuharov, Riv. Nuovo Cim. **38** (2015) 449

[9] M. Battaglieri *et al.*, arXiv:1707.04591 (2017)

[10] G. Mazzitelli *et al.*, Nucl. Instrum. Methods A 515 (2003) 524

[11] P. Valente *et al.*, arXiv:1603.05651 (2016)

[12] R. Assiro *et al.*, Nucl. Instrum. Methods A 898 (2018) 105

[13] F. Ferrarotto *et al.*, IEEE Trans. Nucl. Sci. 65 (2018) 8

[14] S. Ivanov and V. Kozhuharov, AIP Conf. Proc. 2075 (2019) 080005

[15] A. Frankenthal *et al.*, Nucl. Instrum. and Methods A 919 (2019) 89

[16] M. Raggi and V. Kozhuharov, Adv. High Energy Phys. 2014 (2014), 959802

[17] B. Adeva *et al.*, Nucl. Instrum. Methods A 289 (1990) 35

[18] https://www.gestionesilo.it/

[19] http://www.ggg-tech.co.jp/maker/eljen/ej-500.html

[20] http://www.ggg-tech.co.jp/maker/eljen/ej-510.html

[21] http://www.hzcphotonics.com/en_introduction%20of%20products.html

[22] G. F. Knoll, *Radiation Detection and Measurement*, 4^{th} *edition* (2010), ISBN 978-0-470-13148-0

[23] https://www.caen.it/products/v1742/

[24] E. Leonardi *et al.*, J. Phys. Conf. Ser. 898 (2017) 032024

[25] M. Raggi *et al.*, Nucl. Instrum. Methods A 862 (2017) 31

[26] E. Leonardi, G. Piperno and M. Raggi J. Phys. Conf. Ser. 898 (2017) 072019